Title

Dopant Mediated Assembly of Cu_2ZnSnS_4 Nanorods into Atomically Coupled 2D Sheets in Solution.

Journal

Nano letters, 17(6)

ISSN

1530-6984

Authors

Singh, Ajay
Singh, Amita
Ong, Gary K
et al.

Publication Date

2017-06-01

DOI

10.1021/acs.nanolett.7b00232

Peer reviewed

NANO LETTERS

Letter

pubs.acs.org/NanoLett

Dopant Mediated Assembly of Cu_2ZnSnS_4 Nanorods into Atomically Coupled 2D Sheets in Solution

Ajay Singh,[†,‡,○] Amita Singh,[†,‡,○] Gary K. Ong,[†,§] Matthew R. Jones,[∥] Dennis Nordlund,[▽] Karen Bustillo,[‡] Jim Ciston,[‡] A. Paul Alivisatos,[§,∥,⊥,#] and Delia J. Milliron*[,†]

[†]McKetta Department of Chemical Engineering, The University of Texas at Austin, 200 East Dean Keeton Street, Austin, Texas 78712, United States

[‡]National Center for Electron Microscopy, Molecular Foundry, Lawrence Berkeley National Laboratory, 1 Cyclotron Road, Berkeley, California 94720, United States

[§]Department of Materials Science and Engineering, University of California—Berkeley, Berkeley, California 94720, United States

[∥]Department of Chemistry, University of California—Berkeley, Berkeley, California 94720, United States

[⊥]Materials Sciences Division, Lawrence Berkeley National Laboratory, Berkeley, California 94720, United States

[#]Kavli Energy NanoScience Institute, Berkeley, California 94720, United States

[▽]Stanford Synchrotron Radiation Lightsource, P.O. Box 20450, Stanford, California 94309, United States

Supporting Information

ABSTRACT: Assembly of anisotropic nanocrystals into ordered superstructures is an area of intense research interest due to its relevance to bring nanocrystal properties to macroscopic length scales and to impart additional collective properties owing to the superstructure. Numerous routes have been explored to assemble such nanocrystal superstructures ranging from self-directed to external field-directed methods. Most of the approaches require sensitive control of experimental parameters that are largely environmental and require extra processing steps, increasing complexity and limiting reproducibility. Here, we demonstrate a simple approach to assemble colloidal nanorods *in situ*, wherein dopant incorporation during the particle synthesis results in the formation of preassembled 2D sheets of close-packed ordered arrays of vertically oriented nanorods in solution.

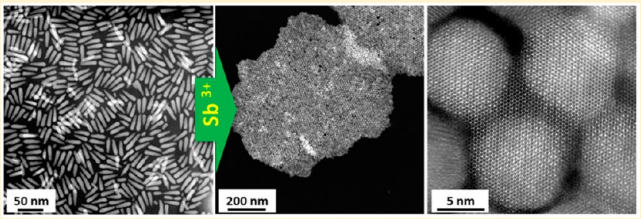

KEYWORDS: *Nanocrystals, nanorods, self-assembly, dopants, phase-transition*

The ordered assembly of anisotropic nanocrystals into macroscopic superstructures is one of the most challenging hurdles for bottom-up routes to three-dimensional (3D) hierarchically structured arrays with tailored optoelectronic properties.[1−4] These superstructures have novel properties that arise not only from the intrinsic characteristic of nanocrystal building blocks but also from their interactions when closely coupled physically and electronically.[1,4−6] Thus, properties can be tuned precisely both by controlling nanocrystal type (shape, size, crystal structure, and composition) and/or by controlling organization of the superstructure.[4,6−8] Potential applications in devices such as lasers, solar cells, and light-emitting diodes (LEDs) further motivate research to understand and control the process of assembly.[1,4,8]

Compared with assembly of spherical nanocrystals, understanding the assembly of anisotropic nanocrystals into ordered arrays is more complex due to the reduced symmetry in their interactions and associated limited tolerance for shape and size polydispersity.[1−3] Spherical nanocrystals have been extensively studied as building blocks for single and multicomponent superstructures where assembly outcomes depend mainly on nanocrystal size ratios due to their isotropic interactions.[8] Recent advances in the colloidal synthesis of nanocrystals that offer robust control over shape (rods, tetrapod, plate, octopod, etc.), size, crystal structure, and composition (binary, ternary, quaternary, etc.) enable exploration of anisotropic nanocrystal superstructures and fabrication of new form factors of hierarchical structures.[8] Nanorods present particular interest due to their inherent length- and shape-dependent properties (linearly polarized emission, stark effect, and band gap), while assembled superstructures of nanorods can further augment their inherent properties for device applications ranging from catalysis, LEDs, photonics, and solar cells.[1,9−11] For example, in solar cell applications, a superstructure containing oriented nanorods (or their heterojunction) could minimize carrier recombination by providing a direct electron transport pathway through the long axis, while the radial axis allows efficient electron−hole pair separation.[10−12]

Received: January 17, 2017
Revised: April 26, 2017
Published: May 9, 2017

DOI: 10.1021/acs.nanolett.7b00232
Nano Lett. 2017, 17, 3421−3428

Assembling anisotropic nanostructures into columnar arrays with both smectic and nematic phases from colloidal solution has been achieved by exploiting various inherent and external forces such as inter-rod van der Waals, dipole−dipole, electrostatic, template/substrate directing, solvation/depletion forces, and external magnetic or electric fields.[2,3,11−25] For example, both vertical and lateral assembly of colloidal nanorods over centimeter scale have been shown for simple binary to complex quaternary (CdS, CdSe, CdSe/CdS, $CuIn_{1-x}Ga_xS_2$, etc.) materials using either drying mediated self-assembly or external fields.[2,11−28] In most cases, self-assembly approaches are dependent upon various critical parameters (nanorod concentration, solvent, temperature, charge, drying rate), which are hard to control precisely and are also time-consuming and subject to experimental uncertainties.[2,14,16−19,22,23] Assembly of nanorods as clusters in solution has been investigated previously via postsynthetic modifications such as the introduction of organic or polymer additives or nonsolvent, which can interfere with device properties.[13,25,26] Ideally, a preferred approach should be additive free yet yield assembled nanorods in solution that can be cast via conventional techniques into oriented, assembled thin films thus allowing simple incorporation of a superstructure into nanocrystal devices.

Here, we present a simple route where incorporation of foreign ions or dopants in the Cu_2ZnSnS_4 (CZTS) nanorod structure induces self-assembly of nanorods into 2D sheets of vertical nanorod arrays in solution during synthesis without isolation of the nanorods from the reaction or using any applied external fields, solvent evaporation, and templating additives. Furthermore, the dispersed solution containing the 2D sheets can be deposited on any substrate by solution processing to form thin films of micrometer-sized oriented nanorod superlattices. We found that dopant incorporation in the nanorods modifies their surface chemistry, which triggers the formation of 2D sheets in solution that further fuse via covalent bonding between nanorods (on side facets), leading to extended structures with preserved orientation. Detailed structural characterization using small-angle X-ray scattering (SAXS) and aberration-corrected electron microscopy demonstrates that nanorods self-assembled into vertically aligned nanorod superlattice monolayer sheets in solution. The CZTS nanorods were synthesized in the wurtzite phase,[27] which is a metastable phase in these materials, and their self-assembled sheets were shown to undergo a metastable-to-stable phase transition during thermal treatment into kesterite (stable phase)[28] to form extended planar crystals of oriented kesterite thin films. Further, antimony has been deliberately selected as a dopant as it has been previously shown that it acts as a grain growth promoter during annealing or selenization/sulfurization in thin films and nanocrystals of copper-based chalcogenide compound semiconductors.[29−32] The observation of dopant-triggered self-assembly leads to mechanically robust nanorod sheets with a high degree of crystallographic ordering, which may enable efficient charge transport with wide-reaching applications such as photocatalysis and photovoltaics.

Wurtzite phase CZTS nanorods were prepared by a high-temperature colloidal chemical synthesis route (see Supporting Information for details).[27] Figure 1a shows an annular dark-field scanning transmission electron microscope (ADF-STEM) image of the uniform nanorods. The nanorods are highly crystalline (Figure S1a) and defect-free, having wurtzite structure (XRD Figure S1b) with elongation along the [002] direction. The selected-area electron diffraction (SAED) pattern (inset in Figure 1a) is indexed to the hexagonal phase. By holding constant

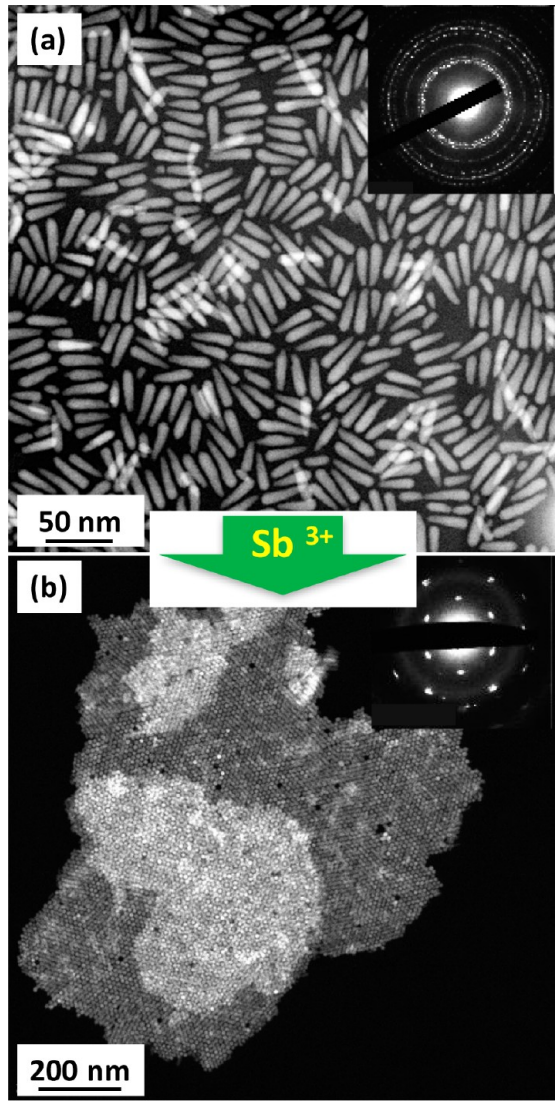

Figure 1. ADF-STEM images of (a) CZTS NRs and (b) Sb-doped CZTS 2D sheets. Inset shows the SAED patterns, respectively.

all synthetic variables with the exception of dopant (antimony) presence in the reaction medium, the resulting colloidal solution was controlled to contain either dispersed nanorods or two-dimensional (2D) supercrystal sheets of nanorods assembled with their long axes perpendicular to the plane of the sheets.

Figures 1b and S2a,b (low magnified) show the ADF-STEM images of typical 2D sheets of nanorods. The inset SAED pattern (Figure 1b) clearly demonstrates the resultant crystallographic alignment of the nanorods in the 2D sheets. These sheets, when deposited on the substrate, show the formation of Moiré interference patterns (Figure S2c,d), which results from overlapped sheets having rotational offsets. The occurrence of Moiré patterns in assembled 2D sheets further demonstrates the extraordinary order of the constituent nanorods.[33] The unidirectional orientation of nanorods in the entire sample of nanosheets was further supported by X-ray powder diffraction (XRD). The diffraction peak intensity in the XRD pattern is strongly dependent upon the relative orientation of lattice planes. The XRD pattern of 2D sheet shows an intense (002) peak (Figure S3), indicating that the (002) planes tend to lie perpendicular to the substrate. The relative intensities of the XRD peaks confirms the preferential orientation of nanorods (perpendicular to the

DOI: 10.1021/acs.nanolett.7b00232
Nano Lett. 2017, 17, 3421−3428

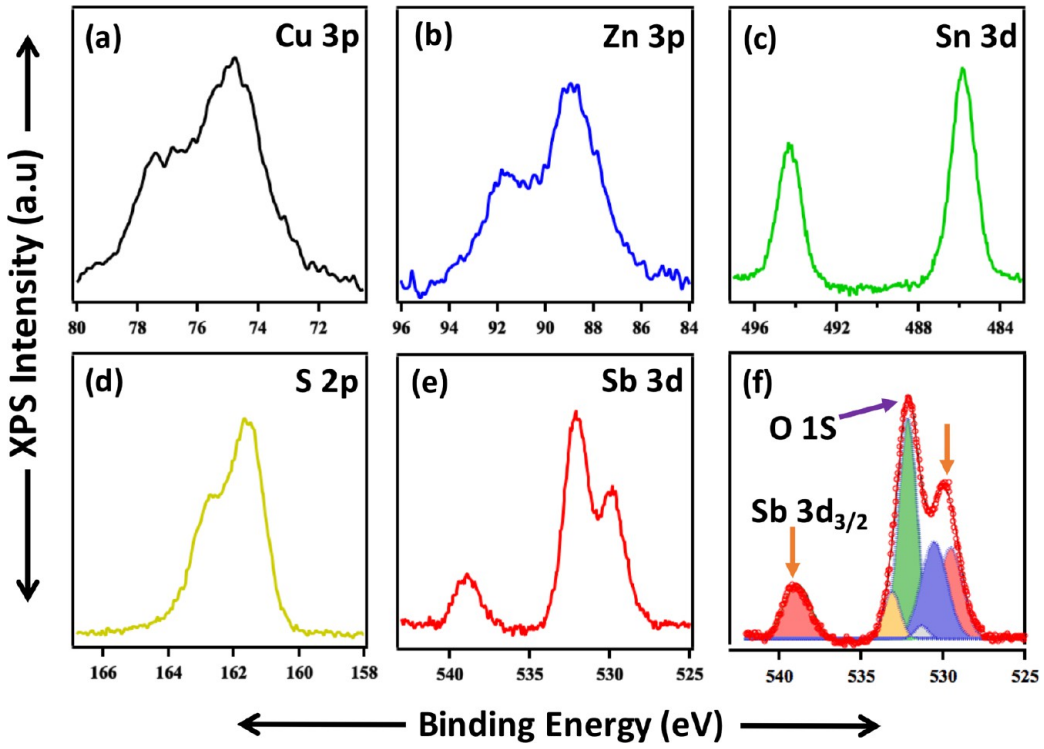

Figure 2. (a–e) High-resolution scans of antimony (Sb) doped CZTS 2D sheets using 650 eV incident photon energy. (f) High-resolution scan of antimony (Sb) and overlapping oxygen region showing the fitted components used to extract the subshell (Sb 3d) contribution.

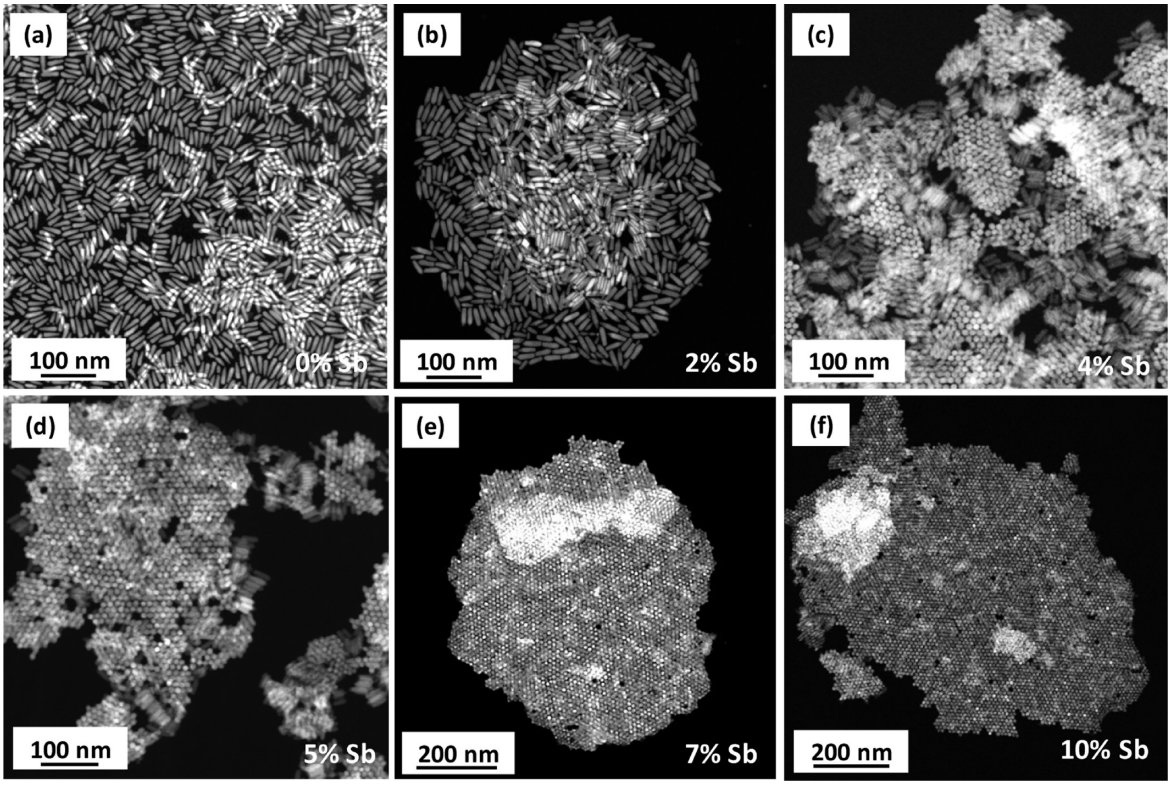

Figure 3. (a–f) ADF-STEM images show the effect of dopant concentration (from 0% to 10%) on the formation of 2D sheets.

plane of the substrate) enforced by the incorporation into nanosheets, which tend to lie flat on the substrate.[17−19] Further analysis of the XRD pattern shows that the thin film composed of 2D sheets contains 89 ± 4% of nanorods oriented along the (002) direction (see detail in SI).

The 2D sheets were further characterized for compositional homogeneity using energy dispersive X-ray spectroscopy (EDS) mapping and X-ray photoelectron spectroscopy (XPS). The EDS maps confirm the homogeneous presence of Cu, Zn, Sn, and S (Figure S4). It was difficult to generate an EDS map to locate the

DOI: 10.1021/acs.nanolett.7b00232
Nano Lett. 2017, 17, 3421−3428

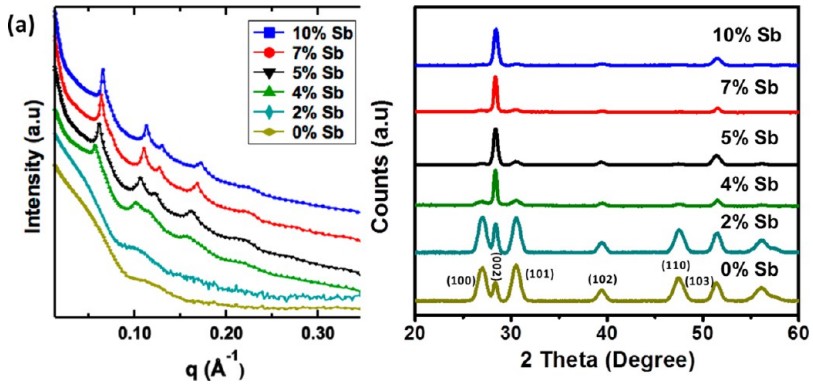

Figure 4. (a) Solution SAXS and (b) XRD of CZTS nanorod synthesis using varying dopant concentration.

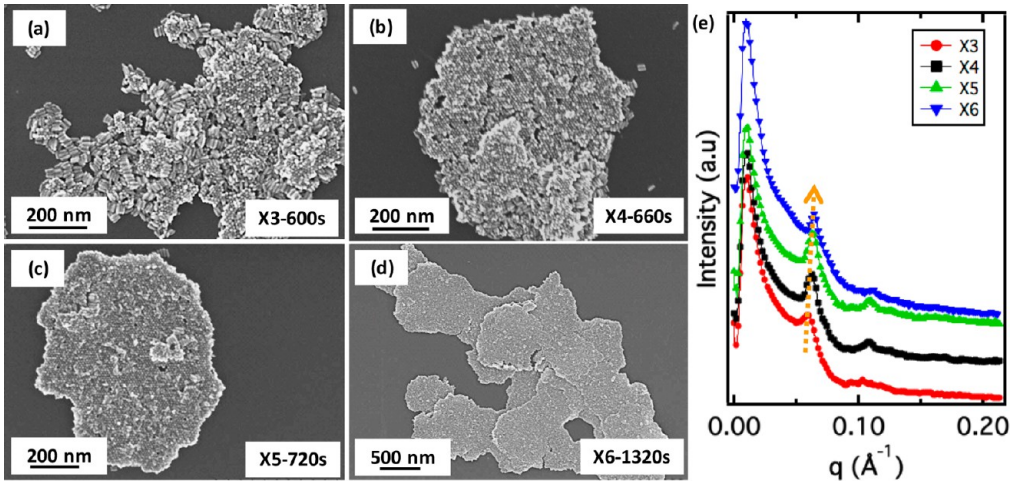

Figure 5. (a–d) Low-resolution SEM images of the aliquot taken during the synthesis revealed the growth mechanism of sheets. (e) SAXS pattern shows the ordered 2D hexagonal structure.

Sb incorporation due to the weak Sb K-edge and the overlapping Sb L-edge and Sn L-edges peaks (see detail discussion in Figure S4a). To overcome this difficulty, we used XPS to investigate the Sb incorporation in 2D sheets. XPS analysis shows the presence of Sb in the 2D sheet, along with the other elements (Cu, Zn, Sn, and S, see survey spectra in Figure S5a) for which the oxidation states are as expected for this composition. The observed binding energy of the peaks for the elements (Cu, Zn, Sn, and S) agree well with previously reported oxidation states of the individual elements in CZTS nanocrystals (Cu^{+}, Zn^{2+}, Sn^{4+}, and S^{2-}, respectively) (Figure 2a–f).[26,27] For antimony (dopant), we analyzed the Sb 3d spectra and observed a typical 3d doublet (Figure 2g) and also found that the Sb $3d_{3/2}$ spectral peak is at 539.02 eV, which is attributed to Sb^{3+} oxidation state (Sb^{4+} and Sb^{5+} have peaks closer to 540 eV) and matches well with the published literature on Sb based materials.[34,35] In addition to confirming the presence of Sb in the sheets, we have also performed XPS depth analysis using energy-dependent synchrotron radiation at the Stanford Linear Accelerator Center, which allows variation of the escape depth of the photoemitted electrons.[36,37] These measurements revealed that the nanorod surface is Sb rich (see detailed discussion in SI).

To validate the role of antimony as a dopant in the sheet formation process, we systematically tuned the amount of antimony precursor [$Sb(ac)_3$] while keeping all other reaction and purification conditions constant. Figure 3 shows the ADF-STEM images of the resulting nanocrystals synthesized with different dopant amounts as defined by the amount in the precursor; sheet evolution of the doped nanocrystals is evident in these images. At a low concentration of dopant (~2%, see detail in SI), there is no sign of sheet formation, as the nanorods are randomly lying on the substrate similar to the undoped case. Further increase of the dopant concentration to 4% results in regions that contain a small number of nanorod assemblies (bundles) in the side-by-side fashion lying perpendicular to the substrate, as seen in Figure 3c. The first indication of 2D nanorod sheet formation begins at a Sb concentration of around 5%. However, as shown in Figure 3d, the formation of 2D sheets is accompanied by the formation of small nanorod bundles and unassembled nanorods. As the dopant concentration is increased to 7 and 10%, the solution consists only of 2D sheets of nanorods with no unassembled nanorods (Figure 3e,f).

To shed light on the effect of dopant incorporation on the formation of nanorod sheets, we applied solution SAXS in transmission geometry to samples with increasing dopant quantities (Figure 4a). Due to the random orientation of individual sheets in solution, the scattering patterns were isotropic, so we chose to analyze 1D patterns obtained via azimuthal averaging of representative 2D data.[38−40] When the dopant quantity was low or absent, the scattering spectra consisted only of the nanorod form factor with periodic undulations characteristic of nanorods with uniform widths. As the dopant amount was increased to 4% and beyond, Bragg peaks emerged with the primary peak occurring at ca. 0.065 $Å^{-1}$. This

DOI: 10.1021/acs.nanolett.7b00232
Nano Lett. 2017, 17, 3421−3428

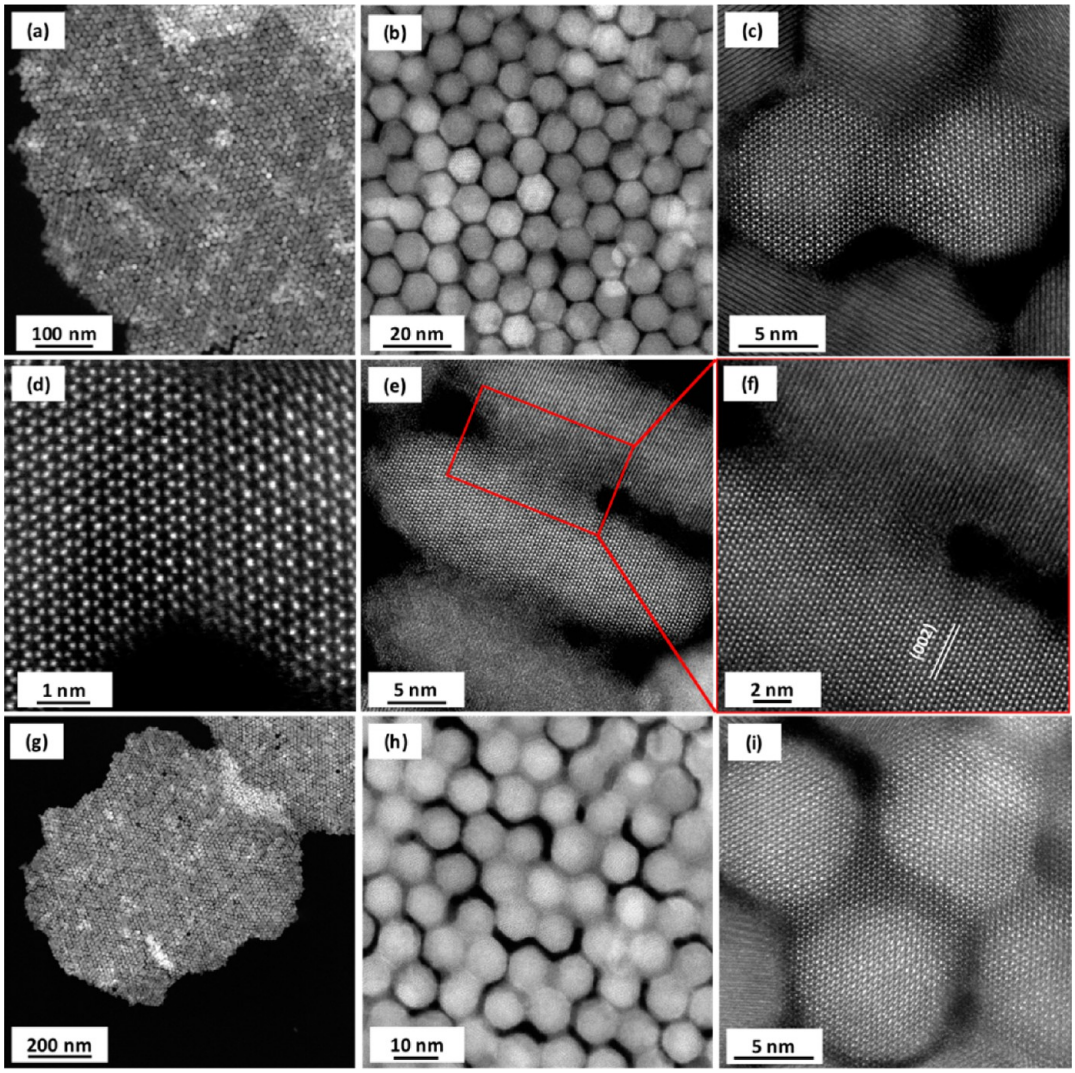

Figure 6. (a–d) Low and high magnification HAADF-STEM images of 2D sheets along the [001] direction. (e,f) High-resolution HAADF-STEM images of the interface of coupled nanorods viewed along the [010] direction. (g–i) Low and high magnification HAADF-STEM images of 2D sheets obtained after a longer reaction time than is typical.

peak position translates to an approximate internanorod distance of 11 nm; the q-spacing ratios of higher order peaks obey 1, $\sqrt{3}$, $\sqrt{4}$, and $\sqrt{7}$ ratios confirming that the nanorods are assembling in a 2D hexagonal lattice.[38,39] Beyond 4%, the Bragg peak shapes sharpen indicating formation of larger, more ordered arrays. To confirm that these nanorod sheets remain as single planar sheets without stacking in solution, we also examined the solutions at a lower q range commensurate to the nanorod length, but found no additional scattering features aside from the nanorod form factor. Further XRD analysis of CZTS nanorods with varying Sb concentrations also confirmed the 2D sheet formation. Figure 4b shows that XRD patterns for the sample with Sb concentration beyond 4% have an increased (002) diffraction peak intensity (crystal plane lying perpendicular to the substrate), while the intensity from (100) planes (crystal plane lying horizontal to the substrate) decreased,[15−17] which clearly agrees with the SAXS analysis (Figure 4a).

During the synthesis, aliquot studies were performed for 7% Sb to investigate the nanocrystal growth and subsequent assembly process. Similar to previous reports on the growth mechanism of compound semiconductor nanocrystals (CIS/Se, CIGS/Se, CIZS, etc.), CZTS nanocrystal formation began with the formation of spherical NCs of copper sulfide (Figure S6-X1, see detail in SI), and as the reaction proceeded, the anisotropic nanorod shape (Figure S6-X2) evolved with the incorporation of other metal ions.[22,37,41,42] As the growth proceeded, small clusters of aligned nanorods nucleated, which grew into larger sheets as shown in Figure 5a–d [(X3 to X6) (Note: 2D sheets are formed during synthesis (not postsynthetically), and there is no effect of purification/washing; Figure S7 shows the STEM images of unwashed product, which clearly indicate the presence of 2D sheets in the reaction product)]. By monitoring this process with solution SAXS on aliquots (Figure 5f), we found that the internanorod distance decreases with reaction time (the peak around 0.01 $Å^{-1}$ in Figure 4f is due to beam stop), with a net reduction of ca. 0.8 nm (see detail in SI for conversion of d-spacing to internanorod distances). This distance is comparable to the ligand length on the nanorod surface.

A complete mechanistic understanding of the role of Sb^{3+} in the nanosheet formation remains elusive, but X-ray photoelectron spectroscopy (XPS) provides some important insights. XPS analysis on the aliquots shows that there is no Sb^{3+} incorporation on the nanorods (X2, Figure S8) before the appearance of nanorod clusters. However, it shows the presence

DOI: 10.1021/acs.nanolett.7b00232
Nano Lett. 2017, 17, 3421−3428

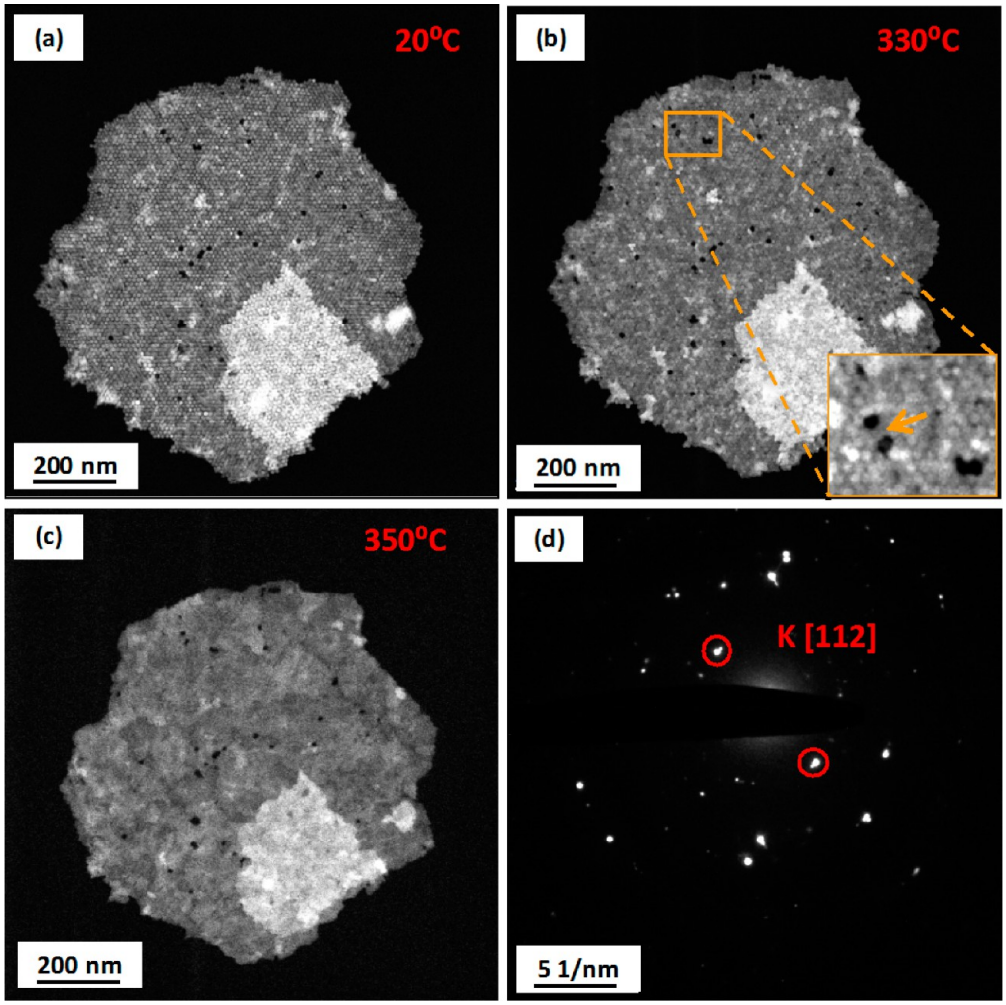

Figure 7. (a–c) ADF-STEM images of 2D sheet at different temperatures during annealing experiment. (d) SAED pattern of the final crystal structure after complete phase-transformation.

of Sb^{3+} in the later aliquot (X3, Figure S8), where the first nucleation of the aligned nanorod clusters was observed. This was the first indication that Sb doping is directly involved in inducing the nanosheet formation. To further validate this hypothesis, the dopant precursor was introduced in the reaction mixture during the later stage of the synthesis (after the nanorods were fully formed), which also resulted in the formation of 2D sheets (see further details in SI, Figure S9a–c). Further, thermal gravimetric analysis (TGA) shows that doped 2D sheets have lower ligand density (~12%) than undoped (~20%) nanorods (Figure S10), which suggests that dopant incorporation at the nanorod surface influences their surface chemistry, leading to nucleation of the assembly of nanorod clusters. We hypothesize that Sb incorporation on the nanorod surface modifies the ligand density due to the change in the local chemical composition at the nanorod surface. For example, based on Hard Soft Acid Base (HSAB) theory, Sb^{3+} is a borderline Lewis acid, and the binding with the thiol ligand (soft base) will be less favorable than for Cu^{+} (soft acid). Strong binding between Cu^{+} and thiols is well-known[43] and thiols are commonly used as ligands for multinary Cu chalcogenide nanocrystals[44] similar to CZTS. Additional synthesis was carried out using a different dopant precursor ($SbCl_3$ instead of $Sb(ac)_3$), and indeed, 2D sheets were formed (Figure S11). This observation strongly suggests that antimony itself is instigating agent for assembly.

We next investigated the bonding between nanorods. Interestingly, 2D sheets were very difficult to dissociate even with 5–7 h-long sonication; it was necessary to use a tip sonicator with high power for 1–2 h to break apart the 2D sheets. When the sheets did finally break apart, they did so by breaking into small clusters and not by separating into individual nanorods. This observation suggests that the nanorods are either held together by very strong and short-range interparticle forces or they are directly connected with strong inorganic bonds. To investigate further, we used aberration-corrected scanning transmission electron microscopy (STEM) of 2D sheets along the [001] axis (Figure 6). Figure 6a,b shows low and high magnification images of a sheet, where vertical orientation of nanorods is clearly visible; it is apparent in these images that most of the nanorods are fused together. Further image magnification of the sheets revealed that the nanorods are indeed coupled by direct inorganic bonds (Figure 6c). Atomic resolution images of the interface show that the coupling occurs among the (100) crystallographic surface terminating planes of the isolated rods with fully epitaxial interfaces (Figure 6d). Coupling of nanorods can be further supported by comparing the SAXS patterns of the aliquots (Figure 5e), where the intensity of the peak increases first (X3) but decreases in the final aliquot (X6). The initial increase is likely due to enhanced ordering leading to additional contribution from Bragg scattering, while the later decrease may

DOI: 10.1021/acs.nanolett.7b00232
Nano Lett. 2017, 17, 3421–3428

be ascribed to fusion of the nanorods that reduces the scattering contrast between the internanorod space and the actual nanorod. While it is clear that the nanorods are coupled together, the extent of coupling along the rod length is difficult to see in the images (Figure 6c,d), as the nanorods are vertically oriented in the 2D sheet.

In order to observe the fused region in a perpendicular direction along the [010] zone axis, we investigated the aliquot sample where the first nucleation of nanorod clusters happens. In this aliquot, some of the nascent nanorod clusters are lying flat on the surface, giving access to additional viewing directions ([210], [110]). High-resolution HAADF-STEM images (Figure 6e,f) clearly show that the nanorods are coupled in these early stages of growth. Hence, we believe that sheet formation proceeds via the following two steps: (i) small clusters of aligned nanorods are nucleated during dopant incorporation in the late stages of nanorod growth, and (ii) nanorod sheets grow from these clusters by displacement of the internanorod ligands and by partial fusion of the nanorods using the unreacted monomers present in the reaction. This has been further confirmed by comparing the HAADF-STEM images of sheets grown for the typical reaction time (15−30 min, Figure 6a,b) vs a longer reaction time (60−90 min); indeed, the sheets apparently fuse to a greater extent with a longer reaction time (Figure 6g−i). This evolution suggests the premise that the remaining unreacted monomers play a crucial role as a source for the material that progressively fuses the nanorods. Furthermore, when the undoped CZTS nanorod reaction is allowed to proceed longer, there is no 2D sheet formation (Figure S12a,b), which confirms that the assembly and fusing are triggered by the incorporation of dopants at the nanorod surface. Similar coupling/bridging with both isotropic and anisotropic nanostructures has been showed recently.[5,6,22,37]

As mentioned earlier, these CZTS nanorods are synthesized in a metastable phase, so their preferential assembly into 2D sheets can be further exploited to form extended planar crystals of the stable phase, kesterite, upon thermal treatment. Due to its nearly isotropic structure, kesterite nanocrystals would be difficult to directly synthesize or assemble in an anisotropic morphology (such as nanorods). An *in situ* TEM heating experiment was carried out using a Gatan single tilt heating stage (see detail in SI), which allowed direct observation of morphological evolutions during the phase transformation. Figure 7a shows an ADF-STEM image of a 2D sheet before annealing, where the preferential orientation of the nanorods is clearly visible. Increasing the temperature up to 300 °C in 30 min showed no indication of phase-transformation or visible change in the 2D sheets. As the temperature was ramped gradually to 360 °C, the nanocrystals began transforming into the kesterite phase around 330 °C, resulting in the coalescence of nanorods (in some parts) as shown in the inset of Figure 7b (close-up region in orange box). The region of the sheet that did not undergo a phase transformation still exhibited hexagonal packing of nanorods (Figure 7b). As the temperature reached 350 °C, transformation of the nanorod sheet was complete (Figure 7c). This planar oriented kesterite structure transformation is clearly revealed by electron diffraction in Figure 7d, where the spots can be indexed to kesterite phase (stable phase) for this compound semiconductor. The absence of wurtzite diffraction spots indicates complete transformation. In-depth inspection of Figure 7b−d and the video collected from other studies carried out by our group on these materials using *in situ* XRD and differential scanning calorimetry (to be published separately) shed more light on the transformation mechanism. The high-energy facets at the nanorod tips apparently facilitate nucleation, and grain growth propagates the transformation into neighboring nanorods (due to close packing in the sheets). This synthesis route ultimately leads to the formation of thin films of kesterite as grain growth is concluded. These thin films of compound semiconductor are highly desirable for solar cells, and exploiting these alternative routes to form orientation-controlled thin films will be beneficial for solar cell and other optoelectronic technologies.

In summary, we have shown that anisotropic nanocrystals, specifically CZTS nanorods, can be assembled in solution during synthesis by the incorporation of dopants in the reaction mixture. The dopant not only incorporates into the nanorods but also influences their surface chemistry, which triggers the coupling and fusing of the nanorods, nucleating an assembly of nanorod clusters. Over the reaction time, these clusters grow, leading to the formation of dispersed 2D nanorod sheets in solution. Formation of these 2D sheets described herein suggests a mechanism to synthesize extended textured thin films of compound semiconductors.

■ ASSOCIATED CONTENT

Supporting Information

The Supporting Information is available free of charge on the ACS Publications website at DOI: 10.1021/acs.nanolett.7b00232.

Full synthetic details, additional HRTEM and ADF-STEM images of nanorod and 2D sheets showing Moiré interference pattern, XRD, XPS, and EDS mapping (PDF)

■ AUTHOR INFORMATION

Corresponding Author

*E-mail: milliron@che.utexas.edu.

ORCID

Ajay Singh: 0000-0002-5168-7522
A. Paul Alivisatos: 0000-0001-6895-9048
Delia J. Milliron: 0000-0002-8737-451X

Present Address

○Materials Physics and Applications Division: Center for Integrated Nanotechnologies, Los Alamos National Laboratory, Los Alamos, New Mexico 87545, United States.

Notes

The authors declare no competing financial interest.

■ ACKNOWLEDGMENTS

This work was performed at the University of Texas at Austin and, in part, at the Molecular Foundry, Lawrence Berkeley National Laboratory, a user facility supported by the Office of Science, Office of Basic Energy Sciences, of the U.S. Department of Energy (DOE) under Contract No. DE-AC02-05CH11231. Some data was collected at beamline 7.3.3 at the Advanced Light Source, which is a DOE Office of Science User Facility under the same contract. Aj.S. was supported by the Bay Area Photovoltaics Consortium, sponsored by DOE EERE. G.K.O. was supported by a National Science Foundation Graduate Research Fellowship under grant number DGE-1106400. Use of the SSRL is supported by DOE under Contract No. DE-AC02-76SF00515. Additional support from the Welch Foundation (F-1848) and the National Science Foundation (CHE-1609656) is gratefully

DOI: 10.1021/acs.nanolett.7b00232
Nano Lett. 2017, 17, 3421−3428

acknowledged. M.R.J. acknowledges the Arnold and Mabel Beckman Foundation for a postdoctoral fellowship.

REFERENCES

(1) Krahne, R.; Morello, G.; Figuerola, A.; George, C.; Deka, S.; Manna, L. *Phys. Rep.* **2011**, *501*, 75−221.
(2) Ryan, K. M.; Singh, S.; Liu, P.; Singh, A. *CrystEngComm* **2014**, *16*, 9446−9454.
(3) Zhang, S.-Y.; Regulacio, M. D.; Han, M.-Y. *Chem. Soc. Rev.* **2014**, *43*, 2301−2323.
(4) Kagan, C. R.; Murray, C. B. *Nat. Nanotechnol.* **2015**, *10*, 1013−1026.
(5) Jia, G.; Sitt, A.; Hitin, G. B.; Hadar, I.; Bekenstein, Y.; Amit, Y.; Popov, I.; Banin, U. *Nat. Mater.* **2014**, *13*, 301−307.
(6) Whitham, K.; Yang, J.; Savitzky, B. H.; Kourkoutis, L. F.; Wise, F.; Hanrath, T. *Nat. Mater.* **2016**, *15*, 557−563.
(7) Peng, X.; Manna, L.; Yang, W. D.; Wickham, J.; Scher, E.; Kadavanich, A.; Alivisatos, A. P. *Nature* **2000**, *404*, 59−61.
(8) Boles, M. A.; Engel, M.; Talapin, D. V. *Chem. Rev.* **2016**, *116*, 11220−11289.
(9) Rizzo, A.; Nobile, C.; Mazzeo, M.; De Giorgi, M.; Fiore, A.; Carbone, L.; Cingolani, R.; Manna, L.; Gigli, G. *ACS Nano* **2009**, *3*, 1506−1512.
(10) Gonzalez-Valls, I.; Lira-Cantu, M. *Energy Environ. Sci.* **2009**, *2*, 19−34.
(11) Rivest, J. B.; Swisher, S. L.; Fong, L.-K.; Zheng, H.; Alivisatos, A. P. *ACS Nano* **2011**, *5*, 3811−3816.
(12) Paik, T.; Diroll, B. T.; Kagan, C. R.; Murray, C. B. *J. Am. Chem. Soc.* **2015**, *137*, 6662−6669.
(13) Talapin, D. V.; Shevchenko, E. V.; Murray, C. B.; Kornowski, A.; Forster, S.; Weller, H. *J. Am. Chem. Soc.* **2004**, *126*, 12984−12988.
(14) Carbone, L.; Nobile, C.; De Giorgi, M.; Sala, F. D.; Morello, G.; Pompa, P.; Hytch, M.; Snoeck, E.; Fiore, A.; Franchini, I. R.; Nadasan, M.; Silvestre, A. F.; Chiodo, L.; Kudera, S.; Cingolani, R.; Krahne, R.; Manna, L. *Nano Lett.* **2007**, *7*, 2942−2950.
(15) Ye, X.; Collins, J. E.; Kang, Y.; Chen, J.; Chen, D. T. N.; Yodh, A. G.; Murray, C. B. *Proc. Natl. Acad. Sci. U. S. A.* **2010**, *107*, 22430−22435.
(16) Singh, A.; Gunning, R. D.; Ahmed, S.; Barrett, C. A.; English, N. J.; Garate, J.-A.; Ryan, K. M. *J. Mater. Chem.* **2012**, *22*, 1562−1569.
(17) Baker, J. L.; Widmer-Cooper, A.; Toney, M. F.; Geissler, P. L.; Alivisatos, A. P. *Nano Lett.* **2010**, *10*, 195−201.
(18) Zanella, M.; Gomes, R.; Povia, M.; Giannini, C.; Zhang, Y.; Riskin, A.; Van Bael, M.; Hens, Z.; Manna, L. *Adv. Mater.* **2011**, *23*, 2205−2209.
(19) Singh, A.; Ryan, K. M. *Part. Part. Syst. Charact.* **2013**, *30*, 624−629.
(20) Singh, A.; Coughlan, C.; Laffir, F.; Ryan, K. M. *ACS Nano* **2012**, *6*, 6977−6983.
(21) Pietra, F.; Rabouw, F. T.; Evers, W. H.; Byelov, D. V.; Petukhov, A. V.; De Mello Donegá, C.; Vanmaekelbergh, D. *Nano Lett.* **2012**, *12*, 5515−5523.
(22) Singh, A.; Coughlan, C.; Milliron, D. J.; Ryan, K. M. *Chem. Mater.* **2015**, *27*, 1517−1523.
(23) Diroll, B. T.; Greybush, N. J.; Kagan, C. R.; Murray, C. B. *Chem. Mater.* **2015**, *27*, 2998−3008.
(24) Singh, A.; English, N. J.; Ryan, K. M. *J. Phys. Chem. B* **2013**, *117*, 1608−1615.
(25) Baranov, D.; Fiore, A.; van Huis, M.; Giannini, C.; Falqui, A.; Lafont, U.; Zandbergen, H.; Zanella, M.; Cingolani, R.; Manna, L. *Nano Lett.* **2010**, *10*, 743−749.
(26) Ramasamy, K.; Zhang, X.; Bennett, R. D.; Gupta, A. *RSC Adv.* **2013**, *3*, 1186−1193.
(27) Singh, A.; Geaney, H.; Laffir, F.; Ryan, K. M. *J. Am. Chem. Soc.* **2012**, *134*, 2910−2913.
(28) Mainz, R.; Singh, A.; Levcenko, S.; Klaus, M.; Genzel, C.; Ryan, K.; Unold, T. *Nat. Commun.* **2014**, *5*, 3133.
(29) Carrete, A.; Shavel, A.; Fontané, X.; Montserrat, J.; Fan, J.; Ibáñez, M.; Saucedo, E.; Pérezrodríguez, A.; Cabot, A. *J. Am. Chem. Soc.* **2013**, *135*, 15982−15985.
(30) Yuan, M.; Mitzi, D. B.; Liu, W.; Kellock, A. J.; Chey, S. J.; Deline, V. R. *Chem. Mater.* **2010**, *22*, 285−287.
(31) Yuan, M.; Mitzi, D. B.; Gunawan, O.; Kellock, A. J.; Chey, S. J.; Deline, V. R. *Thin Solid Films* **2010**, *519*, 852−856.
(32) Tiwari, D.; Koehler, T.; Lin, X.; Harniman, R.; Griffiths, I.; Wang, L.; Cherns, D.; Klenk, R.; Fermin, D. J. *Chem. Mater.* **2016**, *28*, 4991−4997.
(33) Singh, A.; Dickinson, C.; Ryan, K. M. *ACS Nano* **2012**, *6*, 3339−3345.
(34) Garbassi, F. *Surf. Interface Anal.* **1980**, *2*, 165−169.
(35) Moulder, J. F.; Stickle, W. F.; Sobol, P. E.; Bomben, K. D. *Handbook of X-ray Photoelectron Spectroscopy*; Perkin-Elmer, Corp., Physical Electronics Division: Eden Prarie, MN, 1992.
(36) Lounis, S. D.; Runnerstrom, E. L.; Bergerud, A.; Nordlund, D.; Milliron, D. J. *J. Am. Chem. Soc.* **2014**, *136*, 7110−7116.
(37) Singh, A.; Singh, A.; Ciston, J.; Bustillo, K.; Nordlund, D.; Milliron, D. J. *J. Am. Chem. Soc.* **2015**, *137*, 6464−6467.
(38) Li, T.; Senesi, A. J.; Lee, B. *Chem. Rev.* **2016**, *116*, 11128−11180.
(39) Jones, M. R.; Macfarlane, R. J.; Lee, B.; Zhang, J.; Young, K. L.; Senesi, A. J.; Mirkin, C. A. *Nat. Mater.* **2010**, *9*, 913−917.
(40) Burian, M.; Fritz-Popovski, G.; He, M.; Kovalenko, M. V.; Paris, O.; Lechner, R. T. *J. Appl. Crystallogr.* **2015**, *48*, 857−868.
(41) Coughlan, C.; Singh, A.; Ryan, K. M. *Chem. Mater.* **2013**, *25*, 653−661.
(42) Singh, A.; Singh, S.; Levcenko, S.; Unold, T.; Laffir, F.; Ryan, K. M. *Angew. Chem., Int. Ed.* **2013**, *52*, 9120−9124.
(43) Pearson, R. G. *J. Am. Chem. Soc.* **1963**, *85*, 3533−3539.
(44) Zhong, H. Z.; Lo, S. S.; Mirkovic, T.; Li, Y. C.; Ding, Y. Q.; Li, Y. F.; Scholes, G. D. *ACS Nano* **2010**, *4*, 5253−5262.

DOI: 10.1021/acs.nanolett.7b00232
Nano Lett. 2017, 17, 3421−3428